Automatic IVUS segmentation of atherosclerotic plaque with Stop & Go snake

Automatic IVUS segmentation of atherosclerotic plaque with Stop & Go snake

Ellen Brunenberg[1], Oriol Pujol[2], Bart ter Haar Romeny[1], Petia Radeva[2]

[1]Department of Biomedical Engineering, Eindhoven University of Technology,
P.O.Box 513, 5600 MB Eindhoven, the Netherlands

[2]Computer Vision Center, Universitat Autònoma de Barcelona,
Edifici O, Campus UAB, 08193 Bellaterra (Cerdanyola), Barcelona, Spain

e.j.l.brunenberg@student.tue.nl, oriol@cvc.uab.es, b.m.terhaarromeny@tue.nl, petia@cvc.uab.es

Keywords: Intravascular ultrasound, texture features, AdaBoost classification, geodesic active contours

Abstract

Since the upturn of intravascular ultrasound (IVUS) as an imaging technique for the coronary artery system, much research has been done to simplify the complicated analysis of the resulting images. In this study, an attempt to develop an automatic tissue characterization algorithm for IVUS images was done. We concentrated on the segmentation of calcium and soft plaque, because these structures predict the extension and the vulnerability of the atherosclerotic disease, respectively. The first step in the procedure was the extraction of texture features like local binary patterns, co-occurrence matrices and Gabor filter banks. After dimensionality reduction, the resulting feature space was used for classification, constructing a likelihood map to represent different coronary plaques. The information in this map was organized using a recently developed [1] geodesic snake formulation, the so-called Stop & Go snake. The novelty of our study lies in this last step, as it was the first time to apply the Stop & Go snake to segment IVUS images.

1. Introduction

During the last decade, intravascular ultrasound has overtaken angiography as state-of-the-art visualization technique of atherosclerotic disease in coronary arteries. The most important property that determines the occurrence and outcome of acute coronary syndrome is the vulnerability, as opposed to the occlusion. Therefore coronary angiography was not the best method for risk determination, as it displays a shadow of the lumen, without actually imaging the vessel wall and its structures.
Conversely, IVUS images show the morphological and histological properties of a cross-section of the artery. Different plaque tissue types, such as soft or lipid plaque, hard or fibrous plaque, and calcium, can be distinguished. Most significant in a vulnerable plaque is the presence of a large soft core with a thin fibrous cap. Although heavily calcified plaques seem to be more stable than non-calcified plaques, the amount of calcium is an indicator of the overall plaque burden, and as such, the degree of calcification will correlate with the overall risk of plaque rupture in the coronary arterial tree.
Despite the good vulnerability determination, IVUS has the disadvantage that manual analysis of the huge amount of images is difficult, subjective, and time-consuming. Therefore, there is an increasing interest in the development of automatic tissue characterization algorithms for IVUS images. However, this is a challenging problem, as the image quality is poor due to noise, imaging artifacts and shadowing by calcifications.
A lot of research on this question has been done using extraction of texture features to characterize plaque tissues or determine plaque borders [2,3,4,5,6], recently in combination with classification techniques like AdaBoost [7,8]. Deformable models are another extensively used technique to retrieve the intima and adventitia boundaries [9,10,11,12]. Nevertheless, they are not commonly applied to segment different tissue types.
In this study, a new geodesic snake formulation, the so-called Stop & Go snake [1], is employed to find the soft plaque and calcification regions in atherosclerotic plaques. The Stop & Go snake uses likelihood maps to decouple regularity and convergence, thus controlling the role of the curvature in a better way. To ensure convergence, the external force definition is split into an attractive and a repulsive vector field.
We used this new snake in a traditional pattern recognition pipeline: first of all, the extraction of texture features, namely local binary patterns, co-

occurrence matrix, and Gabor filters, was performed on the images. The second stage consists of classification using AdaBoost with decision stumps, addressing soft and fibrous plaque and calcium. The confidence rate map obtained from this classification was used as a likelihood map for the Stop & Go snake.
Those topics are discussed in the following order: section 2 describes the feature extraction and classification. Section 3 discusses the fundamentals of the Stop and Go snake formulation and the use of likelihood maps. Section 4 gives the experimental results and section 5 concludes this paper.

2. Feature extraction and classification

The complexity of IVUS images can be reduced using feature extraction. Because pixel-based gray level-only methods are not sufficient to differentiate between the complicated structures, texture features are used. Examples of the latter discussed in previous studies are co-occurrence matrices and fractal analysis [2], run-length measures and radial profile [4], derivatives of Gaussian, wavelets, Gabor filters, cumulative moments [5], and local binary patterns [6]. Because Pujol et al. achieved best results on IVUS tissue characterization using local binary patterns, co-occurrence matrices, and Gabor filters [5,6], our study was performed using these three features.
After feature extraction, the high-dimensional feature space is used as input for an AdaBoost classifier. The idea behind boosting methods, introduced in 1995 by Freund and Schapire [13], is that many simple, weak classifiers together can form a strong classification algorithm with many practical advantages. AdaBoost is fast, simple, and easy to implement. However, before both feature extraction and classification can be performed, the images have to be preprocessed.

2.1 Preprocessing

The objective of the preprocessing step is twofold: first, some of the images' marks and artifacts, like the legend, calibration marks and the echo of the catheter shaft are removed to avoid their influence on feature extraction and classification. Furthermore, the planar image in Cartesian coordinates is converted into polar coordinates. This is done to prevent biases due to rotation-invariant feature extractors and to simplify processing of the more or less circular vessel structures.

2.2 Feature extractors

With the preprocessed image as input, feature extractors usually give a high-dimensional feature vector as response. The threesome used here, namely local binary patterns, co-occurrence matrices and Gabor filters, all provide a good representation of the texture space for our problem.
The Local Binary Pattern (LBP) operator, introduced by Ojala et al. [14], detects uniform local binary patterns within circularly symmetric neighborhoods of P members with radius R. The basis of this texture operator is the subtraction of the gray value of the center pixel g_c from the gray values of the pixels g_p in the neighborhood. To achieve gray-scale invariance, a value of 1 is assigned if the difference is positive and 0 if negative:

$$s(x) = \begin{cases} 1 & \text{if } x \geq 0 \\ 0 & \text{otherwise} \end{cases}.$$

The values for the whole neighborhood are transformed into one by assigning a binomial factor 2^p to each value and summing the results. From the different output values of this operator, only the rotation-invariant patterns are taken for further

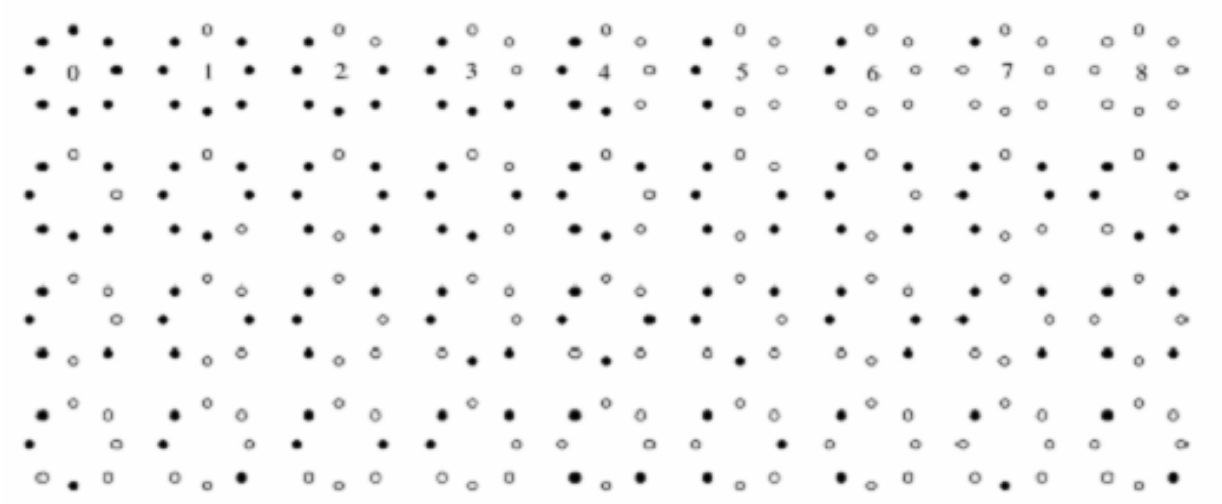

Figure 1: The 36 unique rotation-invariant binary patterns for a neighborhood of 8 pixels.

processing, and among them, there is a minority of local binary patterns that represents the majority of all possible textures. These are called the uniform patterns, because they have only 0 or 2 transitions between 0 and 1 values. They can be found on the first row of figure 1 and are formally defined by a transition counter U, resulting in the following LBP operator:

$$LBP_{P,R}^{riu2} = \begin{cases} \sum_{p=0}^{P-1} s\left(g_p - g_c\right) & \text{if } U\left(LBP_{P,R}\right) \le 2 \\ P+1 & \text{otherwise} \end{cases}.$$

The second feature operator, the gray-level co-occurrence matrix (COOC), provides a statistical tool for extraction of second-order texture information from images [14]. The relative frequencies of gray level pairs of pixels at a certain relative displacement, given by pixel distance D and angle θ, are calculated, stored in the co-occurrence matrix P and then normalized. To achieve a good texture description, four matrices are needed, using the same distance D and four angles, θ = {0º, 45º, 90º, 135º}. After computation of those matrices, the actual feature space is generated by the extraction of six measures from them, namely

$$Energy = \sum_{i,j} P(i,j)^2 ,$$

$$Entropy = -\sum_{i,j} P(i,j) \log P(i,j) ,$$

$$Inverse\ Difference\ Moment = \sum_{i,j} \frac{1}{1+(i-j)^2} P(i,j) ,$$

$$Shade = \sum_{i,j} \left(i + j - \mu_x - \mu_y\right)^3 P(i,j) ,$$

$$Inertia = \sum_{i,j} (i-j)^2 P(i,j) ,$$

$$Pr\,omenance = \sum_{i,j} \left(i + j - \mu_x - \mu_y\right)^4 P(i,j) ,$$

where $P(i,j)$ is the $(i,j)\,th$ element of a normalized co-occurrence matrix, and $\mu_x = \sum_i i \sum_j P(i,j)$ and $\mu_y = \sum_j j \sum_i P(i,j)$.

The last feature operators used for this study are the Gabor filters, originating from the multi-channel filtering theory that describes how the human visual system decomposes the retinal image into a number of filtered images, each with contours on a different scale and in a different direction. A Gabor filter consists of a sinusoidal, modulated in amplitude by a Gaussian envelope. The impulse-response of an even-symmetric Gabor filter is given by

$$h(x,y) = \exp\left\{-\frac{1}{2}\left[\frac{x^2}{\sigma_x^2} + \frac{y^2}{\sigma_y^2}\right]\right\} \cos\left(2\pi u_0 x + \varphi\right) ,$$

where u_0 and φ are the frequency and phase of the sinusoidal along the x-axis and σ_x and σ_y are the scales of the Gaussian along the respective axes. By rotation of the x-y system, filters at different orientations can be obtained. For practical purposes, the angles θ = {0º, 45º, 90º, 135º} suffice again.
To make sure that every feature has an equal influence on the classification result, the extracted feature spaces are normalized.

2.3 AdaBoost classification

The normalized data were classified using our AdaBoost algorithm, with decision stumps or one-level decision trees as weak classifiers. Let the training set contain N samples, consisting of a d-dimensional feature vector $\boldsymbol{x}_i$ (i = 1,…,N) and a class label y_i. Decision stumps threshold these training data using only one out of the d features, assigning a class label based on majority voting [15].
During boosting, such a weak classifier is called repeatedly in a series of rounds t = 1,…,T. The principle of this algorithm is to maintain a distribution of weights assigned to the training samples, denoted by $D_t(i)$. Initially, the samples are classified using equally set weights. In the next round, the weights for incorrectly classified samples are increased, while those for correct observations are reduced. This has the effect that the algorithm focuses on samples misclassified in the previous round, i.e. the difficult samples in the data set [13].

3. Stop & Go snake

In a traditional pattern recognition pipeline, classifiers like AdaBoost are used to find regions of interest after feature extraction. Subsequently, a deformable model can organize the obtained image information.
The deformation of the curve is typically constrained by internal and external conditions, until it adapts to the object of interest. The internal forces influence the continuity and smoothness of the model, while the external conditions are responsible for a good adjustment to the image features.

3.1 Traditional deformable models

The first of the two different kinds of deformable models that can be distinguished are the parametric deformable models that use Newton's mechanics laws to define the internal constraints of the snake, given in terms of snake elasticity and stretch [16].

Because an explicit curve parameterization is used, the model is restricted to single objects.
On the other hand, geodesic active contours have a formulation based on the theory of curve evolution and level sets. A big advantage of this is that it can deal with topological changes during snake evolution. This evolution should find the curve of minimum length in a Riemannian surface with a measure depending on the image gradient. It follows that the snake Γ evolves according to

$$\frac{\partial \Gamma}{\partial t} = \left(g \bullet \kappa - \left\langle \nabla g, \vec{n} \right\rangle \right) \bullet \vec{n} ,$$

with $g = 1/\left(1+\left|\nabla I\right|^2\right)$ and κ the curvature of Γ, $\vec{n}$ its inward unit normal and $\langle , \rangle$ the scalar product of two vectors. It can be seen that the curvature has a double role, defining the motion of the curve at zero gradient regions, but also serving as a curve regularizing term, ensuring continuity. This has the disadvantage that it slows down the numeric scheme because it is a second-order term. Furthermore, it complicates snake convergence into concave areas. To overcome the latter, usually a constant motion term or balloon force V_0 is added:

$$\frac{\partial \Gamma}{\partial t} = \left(g \bullet \kappa + V_0 - \left\langle \nabla g, \vec{n} \right\rangle \right) \bullet \vec{n} .$$

In order to guarantee convergence, its magnitude should be larger than the absolute value of the curvature. However, this requirement makes stopping of the snake on the desired contour difficult, because there, an equilibrium between the velocity V_0 and the vector field ∇g must be achieved [17, 1].

3.2 Stop & Go formulation

To overcome the problems regarding convergence and regularity, a new definition where these terms are decoupled was introduced by Pujol et al. [1]. In this so-called Stop & Go snake, the curvature term does not interfere in the convergence process. The desired decoupling can be achieved using characteristic functions of the region of interest *R*:

$$I(x,y) = \begin{cases} 1 & \text{if } (x,y) \in R \\ 0 & \text{otherwise} \end{cases} .$$

By removing the influence of the curvature, any global vector field properly defining the target contour as its equilibrium ensures convergence. Such a vector field can be split into an exterior attractive field (the Go term) and an inner repulsive one (the Stop term), of which the sum cancels on the curve of interest. The separately defined Go and Stop terms are glued together by means of the characteristic function mentioned above.
If the evolving curve is outside the region of interest *R*, the Go term corresponds to an area minimization process restricted to the outside of *R*. The following equation ensures an inward motion to *R*, comparable to a balloon force:

$$V_{Go} = (1 - I) \bullet V_0 \bullet \vec{n} .$$

Because there is only need for a Stop field in the neighborhood of the desired contour, this term can be defined by the outward gradient *g* locally defining the contours of R:

$$V_{Stop} = I \bullet \left\langle \nabla g, \vec{n} \right\rangle \vec{n} .$$

The Stop and Go snake evolution is then given by:

$$\frac{\partial \Gamma}{\partial t} = \left\langle I \bullet \nabla g, \vec{n} \right\rangle \vec{n} + V_0 \bullet (1 - I) \bullet \vec{n} .$$

Although this formulation leads the curve to the desired boundary of *R*, there is no smoothness and continuity yet. Because these conditions are only required in the final steps of the snake evolution, a restrictive mask $\breve{I}$ can be used to define their scope, here $\breve{I} = G_\sigma * I$, with G_σ a Gaussian filter with standard deviation σ. The equation then becomes:

$$\frac{\partial \Gamma}{\partial t} = \left(I \left\langle \nabla g, \vec{n} \right\rangle + V_0 (1 - I) \right) \vec{n} + \alpha \kappa \breve{I} \vec{n} .$$

In spite of the resemblance of this formula to that of 'traditional' geodesic snakes, the role of the curvature is different here. It is now only a regularizing term of which the influence can be controlled by means of α. Furthermore, it does not trouble the convergence anymore because it only influences the last steps of the evolution.

3.3 Likelihood maps

Unfortunately, for practical applications, there are no characteristic functions defining the regions of interest available, so an alternative function to generate the decoupling is needed.
A likelihood map represents the probability of each pixel to belong to the object of interest. In general, a likelihood map only needs to fulfill the requirement that the object of interest is given as a local extremum. Examples of results that can be used as likelihood maps are the image's direct response to feature extractors or the outcome of the classifier.

The latter is not very suitable, because it has very strong edges that cause the snake to follow simply the contours of this classification map. This is often not the optimal result and besides, there are easier and faster ways to find those edges. In this study, we propose to use the classifier's confidence rates as likelihood maps. These confidence rates can easily be extracted from the AdaBoost classification.
The normalized (between 0 and 1) version of the likelihood map $\breve{L}$ will be used in the Stop & Go snake, leading to:

$$\frac{\partial \Gamma}{\partial t} = \alpha \kappa \breve{L} \bullet \vec{n} + \breve{L} \langle \nabla g, \vec{n} \rangle \bullet \vec{n} + V_0 \left(1 - \breve{L}\right) \bullet \vec{n} \, .$$

Then, the only question remaining is the definition of the Stop term, $\breve{L} \bullet \nabla g$. Pujol et al. [1] proposed to base this term on the likelihood map, defining it as $\nabla \left(1 - \breve{L}\right)$. The formula then becomes:

$$\frac{\partial \Gamma}{\partial t} = \alpha \kappa \breve{L} \bullet \vec{n} + \beta \left\langle \nabla \left(1 - \breve{L}\right), \vec{n} \right\rangle \bullet \vec{n} + V_0 \left(1 - \breve{L}\right) \bullet \vec{n} \, ,$$

with α weighting the role of the curvature and β influencing the smoothness of the curve.

4. Results

The IVUS images used in this study images were acquired by a last generation IVUS scanner (Galaxy, Boston Scientific). Compared to the previous ones, this scanner provides much better contrast and higher resolution, leading to a more expressed texture appearance of all intravascular structures. In this context, the analysis of these images is even more difficult compared to the previous generation images, justifying the texture analysis.
To be able to evaluate the results of the classifier and the Stop & Go snake correctly, they should be compared with a 'ground truth'. For this purpose, IVUS images segmented manually by cardiologists from the Hospital Universitari "Germans Trias i Pujol" in Badalona, Spain, were used.
Furthermore, classifiers like AdaBoost, that perform supervised learning, need a set of training samples. In this study, a set of about 13000 training points, divided over the three tissue types soft plaque, fibrous plaque, and calcium, was selected manually from the cardiologists' segmentation.

4.1 Results of AdaBoost classification

For 30 IVUS images, two classifications were performed using 10 rounds of boosting, one separating fibrous plaque and calcium from soft plaque, and one distinguishing fibrous plaque from calcium. In the classified images shown in column C of figures 2 and 3, it can be seen that calcium and fibrous plaque are classified reasonably well, but that soft plaque apparently is difficult to segment. These observations are confirmed when looking at the confusion matrix in table 1. The majority of soft plaque, fibrous plaque and calcium points are classified correctly, although soft plaque is still repeatedly classified as fibrous. The percentage of points that are assigned correctly is 75.82%.

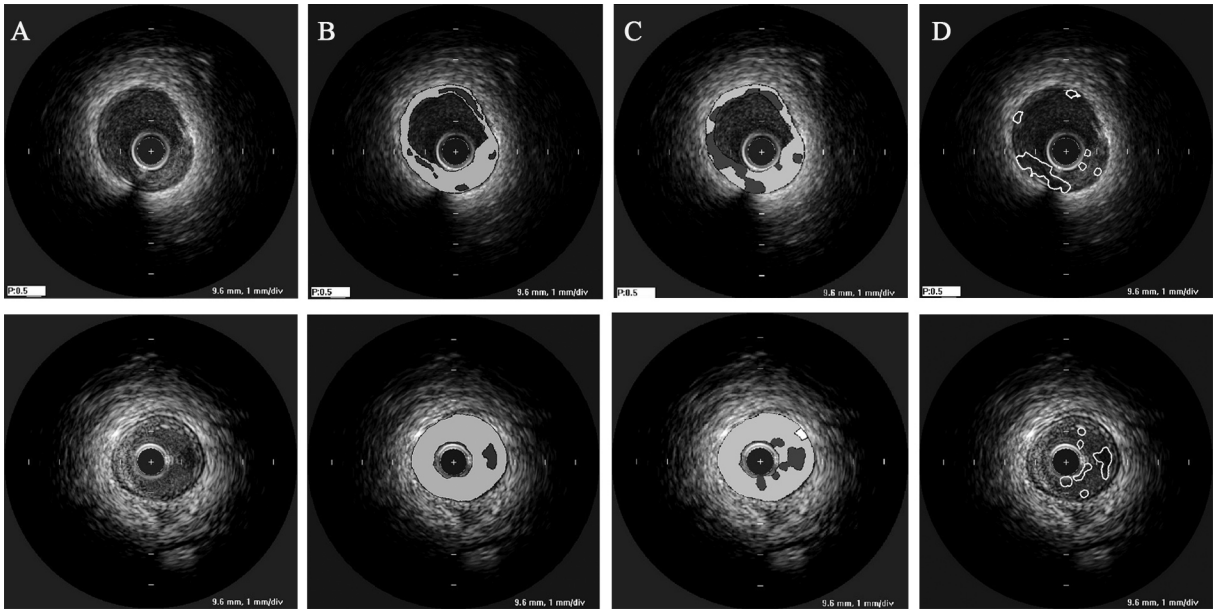

Figure 2: Classification and snake results for two IVUS images with presence of soft plaque. Column A: Original images. B: Images segmented by cardiologist. C: AdaBoost classification map. D: Stop & Go snake result. Legend for columns B and C: Dark gray represents soft plaque, light gray fibrous plaque and white calcification.

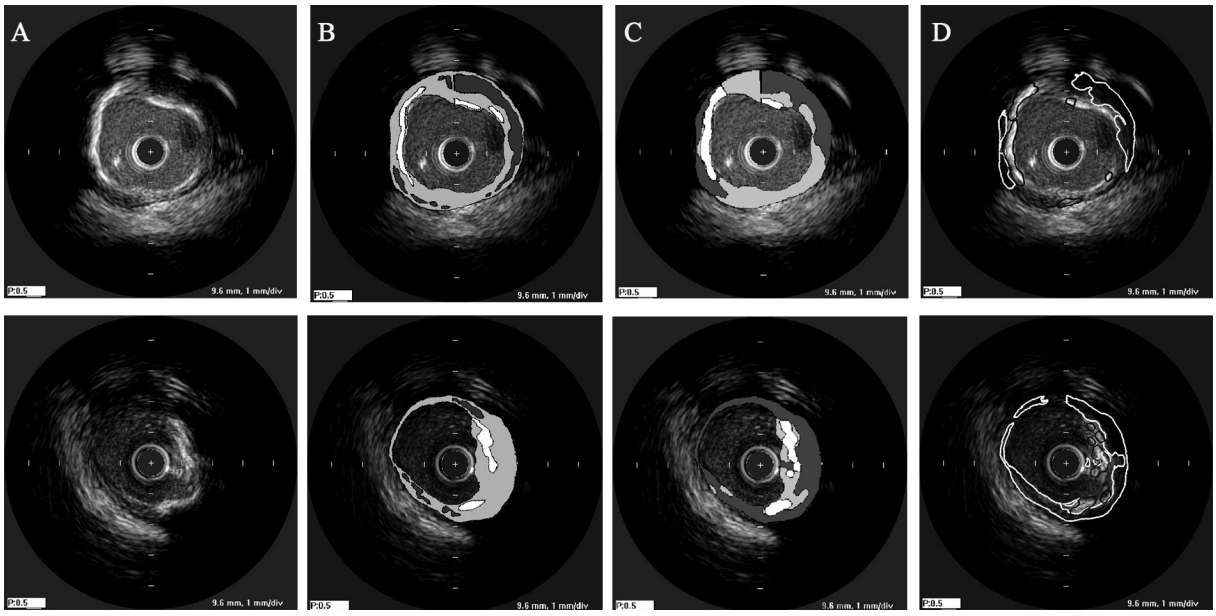

Figure 3: Classification and snake results for two IVUS images with presence of soft plaque and calcium. Column A: Original images. B: Images segmented by cardiologist. C: AdaBoost classification map. D: Stop and Go snake result. Legend for column D: White lines represent soft plaque, black ones calcification.

Table 1: Confusion matrix (in percents) for boosted decision stumps classification for all test images.

	Labeled as soft plaque	**Labeled as fibrous plaque**	**Labeled as calcium**	**Totals**
Classified as soft plaque	5.03	19.11	0.09	24.23
Classified as fibrous plaque	2.43	67.67	0.44	70.54
Classified as calcium	0.00	2.11	3.12	5.23
Totals	7.46	88.89	3.65	100.00

4.2 Results of Stop & Go snake

In addition to the classification map, the AdaBoost classification also gives confidence rates and thresholds as output. Every confidence rate above the threshold represents the probability that the point belongs to the searched class, while a confidence rate below the threshold indicates that the pixel does not belong to this class. In our case, the likelihood map for soft plaque can be derived from the confidence rate map of the first classification, while the map for calcium results from the separation of fibrous plaque and calcium.

For the actual evolution of the snake over the likelihood map, the Level Sets formulation by Osher and Sethian [18] was implemented using an explicit Euler scheme:

$$\varphi_{t+1} = \varphi_t + \left(\alpha \breve{L} \frac{u_{xx}u_y^2 + 2u_{xy}u_x u_y + u_{yy}u_x^2}{|\nabla u|^2} + V_0 \left(1-\breve{L}\right)|\nabla \varphi_t| + \left\langle \nabla\left(1-\breve{L}\right), \nabla \varphi_t \right\rangle \right) \Delta t ,$$

with φ_t the solution at time t, and the derivatives computes using centered finite differences.

Pujol et al. [1] found that the fastest Stop & Go snake configuration uses $\{V_0 = 1.3, \Delta t = 1.3, \text{and } \alpha = 0.23\}$, while a snake fully concerned with accuracy and smoothness uses $\{V_0 = 0.2, \Delta t = 0.5, \text{and } \alpha = 0.6\}$. For this study, the trade-off configuration, to increase convergence speed, was used, being $\{V_0 = 1, \Delta t = 0.5, \text{and } \alpha = 0.6\}$. Furthermore, 300 iteration steps and a β of 150 were applied.

Using those parameters, the Stop & Go snake was applied on all images with soft plaque and calcium. An impression of the behavior during evolution on a calcium likelihood map can be seen in figure 4. The first row contains images taken at 0, 50, and 100 iterations, while the second row displays behavior at 150, 200, and 300 iterations.

After snake deformation, the plaque boundaries found by the cardiologist were superimposed on the mask found for soft plaque or calcium, in order to exclude the catheter and other artifacts. Furthermore, very small regions were omitted. The final output is

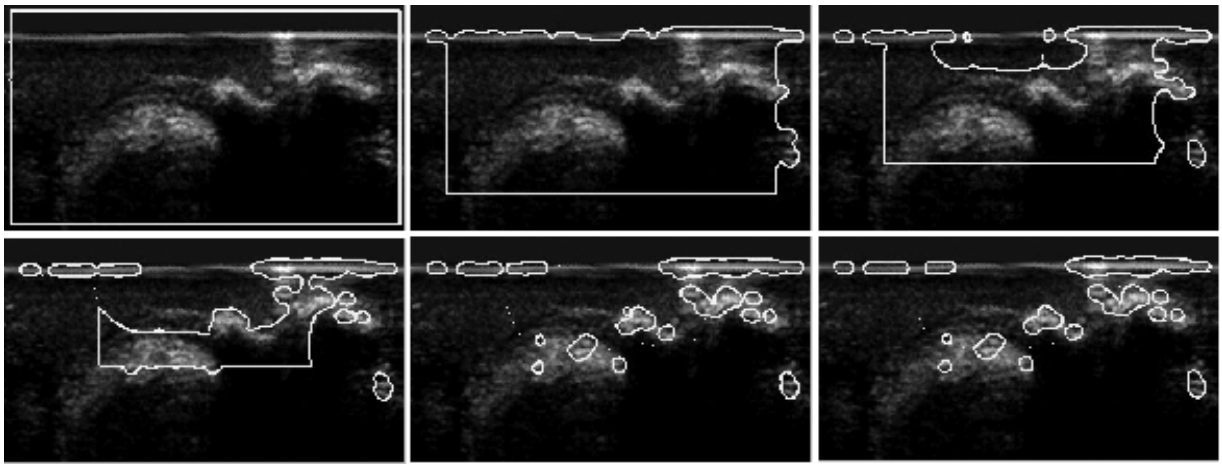

Figure 4: Snake deformation at 0, 50, 100, 150, 200, and 300 iterations.

Table 2: Area comparison for different segmentations and classifications. Remarks: from cardiologist 2, only 8 images with soft plaque and 8 images with calcium were available, and from cardiologist 3, only 8 images with calcium were available, so only those were considered.

'True' mask	**Mask to compare**	**Mean error soft plaque (pixels)**	**Mean error on calcium (pixels)**
Cardiologist 1	Cardiologist 2	4.28 ± 3.45	1.61 ± 0.68
Cardiologist 1	Cardiologist 3	-	1.14 ± 0.65
Cardiologist 1	AdaBoost	5.30 ± 5.08	0.71 ± 0.21
Cardiologist 1	Snake	5.71 ± 5.40	1.86 ± 1.49
AdaBoost	Snake	0.78 ± 0.50	1.06 ± 0.94

mapped on the original images in Cartesian coordinates and is shown in columns D of figures 2 and 3. The white lines indicate the soft plaque found by the snake, while the black represent the calcium.
It can be seen that the selection of soft plaque is weak. However, the calcium detection is reasonable. Unfortunately, it is not trivial to analyze the snake results statistically. In this study, we propose a comparison of the areas of interest found with the snake and the same areas in the cardiologist's segmentation.
We considered 20 images with soft plaque and 8 images with calcium. The error was determined as the area of the regions in the different masks that did not overlap, normalized by the total area of the 'true' mask, for example the cardiologist's map. To get more insight in intraobserver variability and AdaBoost performance as well, five different comparisons were made. The results are in table 2.
As can be seen from the error rates in this table, it is quite difficult to detect soft plaque well, starting with the segmentation of the different cardiologists. The results for calcium are much better. The boosted decision stumps algorithm can be seen to perform better (more similar to the cardiologists 'ground truth') than the snake on finding the regions of interest for this tissue type.

5. Conclusion

In this study, various tools for pattern recognition were considered in an attempt to obtain automatic segmentation of plaque tissues, especially soft plaque and calcium. Different texture features were extracted and the AdaBoost classifier and the Stop & Go snake both performed reasonably well segmenting calcium. These explicit and implicit classification methods both have their advantages and drawbacks. AdaBoost is a little more precise, but considers each point just within its neighborhood. Conversely, the Stop & Go snake organizes points in groups. However, defining the boundary of the region of interest with a proper likelihood map is difficult.
Especially for soft plaque, this step needs special attention in future research. It is important to have an excellent 'ground truth' to base the training set

and the assessment of classifiers' performance on. The intima and adventitia boundaries should be found automatically, using deformable models, for this set of images. Furthermore, classification results should be corrected for shadowing caused by guide wires and calcifications. Finally, an extensive study for other texture feature combinations, different classifiers, and alternative Stop and Go snake parameters configurations could be made.

References

[1] Pujol, O., Gil, D., Radeva, P. Fundamentals of Stop and Go Active Models. Image and Vision Computing, Vol. 23, No. 8, pp. 681-691, 2005.

[2] Nailon, W. and McLaughlin, S. Intravascular ultrasound image interpretation. Proceedings of the International Conference on Pattern Recognition, Austria. IEEE Computer Society Press: USA, pp. 503-506, 1996.

[3] Mojsilovic, A. et al. Automatic segmentation of intravascular ultrasound images: a texture-based approach. Ann. Biomed. Eng. 25, pp. 1059-1071, 1997.

[4] Zhang, X. and Sonka, M. Tissue characterization in intravascular ultrasound images. IEEE Transactions on Medical Imaging, Vol. 17, No. 6, pp. 889-899, 1998.

[5] Pujol, O. and Radeva, P. Automatic segmentation of lumen in intravascular ultrasound images: An evaluation of texture feature extractors. Proceedings for IBERAMIA, pp. 159-168, 2002.

[6] Pujol, O. and Radeva, P. Near real time plaque segmentation of IVUS. Proceedings of Computers in Cardiology, pp. 69-72, 2003.

[7] Pujol, O., Rosales, M. and Radeva, P. Intravascular Ultrasound Images Vessel Characterization using AdaBoost. Functional Imaging and Modelling of the Heart: LNCS 2674, pp. 242-251, 2003.

[8] Pujol, O., Radeva, P., Vitria, J., Mauri, J. AdaBoost to classify plaque appearance IVUS images. Progress in Pattern Recognition, Image Analysis, and Applications: LNCS 3287, pp. 629-636, 2004.

[9] Pujol, O. and Radeva, P. Lumen detection in IVUS image using snakes in a statistical framework. XX Congreso Annual de la Sociedad Española de Ingenería Biomédica, pp. 129-132, 2002.

[10] Roy Cardinal, M.-H., Meunier, J. et al. Intravascular Ultrasound Image Segmentation: A Fast-Marching Method. Medical Image Computing and Computer-Assisted Intervention: LNCS 2879, Vol. 2, pp. 432-439, 2003.

[11] Pujol, O. and Radeva, P. Texture segmentation by statistic deformable models. International Journal of Image and Graphics, Vol. 4, No. 3, pp. 433-452, 2004.

[12] Roy Cardinal, M.-H., Meunier, J. et al. Automatic 3D segmentation of intravascular ultrasound images using region and contour information. Medical Image Computing and Computer-Assisted Intervention: LNCS 3749, Vol. 1, pp. 319-326, 2005.

[13] Freund, Y. and Schapire, R.E. A decision-theoretic generalization of on-line learning and an application to boosting. Journal of Computer and System Sciences, Vol. 55, No. 1, pp. 119-139, 1997.

[14] Haralick, R., Shanmugam, K. and Dinstein, I. Textural features for image classification. IEEE Transactions on System, Man, Cybernetics, Vol. 3, No. 6, pp. 610-621, 1973.

[15] Qu, Y. et al. Boosted decision tree analysis of surface-enhanced laser desorption/ionization mass spectral serum profiles discriminates prostate cancer from non-cancer patients. Supplemental Data. Clinical Chemistry, Vol. 48, No. 10, pp. 1835-1843, 2002.

[16] Kass, M., Witkin, A., Terzopoulos, D. Snakes: active contour models. International Journal of Computer Vision, Vol. 1, No. 4, pp. 321-331, 1988.

[17] Caselles, V., Kimmel, R. and Sapiro, G. Geodesic active contours. International Journal of Computer Vision, Vol. 22, No. 1, pp. 61-79, 1997.

[18] Osher, S. and Sethian, J.A. Fronts propagating with curvature-dependent speed: algorithms based on Hamilton-Jacobi formulations. Journal of Computational Physics, Vol 79, No. 1, pp. 12-49, 1988.